Journal of Intelligent Systems and Internet of Things
Vol. 13, No. 02, PP. 166-177, 2024
DOI: https://doi.org/10.54216/JISIoT.130213

Transfer Learning and Optimised Firefly Neural Network for Lung Cancer

A. Gopinath[1,*], P.Gowthaman[2]

[1]Assistant Professor, Department of Electronics and Communication Science, DRBCCC Hindu College, Pattabiram, Chennai-72, Tamil Nadu, India
[2]Assistant Professor, Department of Electronics, Erode Arts and Science College, Erode, Tamil Nadu, India
Emails: gopinathannamalai76@gmail.com, pg16575@gmail.com

Abstract

Today's clinical analysis and precise illness detection are mandated requirements for the development of intelligent expert systems. Since lung cancer affects both men and women equally and has a greater mortality rate than other illnesses, a more complete examination is needed to diagnose lung cancer. More helpful information regarding a lung cancer diagnosis may be provided by images from a computer tomography (CT) scan. Various machine learning and deep learning algorithms are created to enhance the medical treatment process using CT scan input pictures. But research still has a bad side when it comes to creating a precise and intelligent system. In order to improve the detection of lung tumors from the CT input images, this paper presented Firefly optimized pre trained transfer learning. The previously trained model VGG-16 is used in this paper to extract features more effectively, using the features chosen via the firefly optimization approach to increase classification accuracy while reducing complexity. The thorough testing done with the “LUNA-16 & LIDC Lung image” datasets is assessed & studied along with other performance measures like "accuracy, precision, recall, specificity, and F1-score". Investigation results show that the suggested design outperformed the “DenseNet, AlexNet, Resnets-50, Resnets-100, VGG-16 & Inception models” and reached the top results with "98.5% accuracy, 99.0% precision, 98.8% recall, with 99.1% F1-score.

Received: October 23, 2023 Revised: February 27, 2024 Accepted: June 24, 2024

Keywords: Computer Tomography Images; Firefly Optimization; Vgg16; Classification; Accuracy; Lung Tumor

1. Introduction

Lung Tumor growth is one of the real reasons for death in numerous parts far and wide. GLOBOCAN - which is an undertaking under the International Agency for Research in Cancer (some portion of WHO) that points "to give contemporary assessments of the occurrence of, mortality and commonness from real kind of diseases, at national dimensions, for 184 nations of the world' - announced that lung Tumor is the principal sort of Tumor growth among men and the third for both genders universal. In India, it is the second normal Tumor growth among men and the third when all is said in done with 2100 Indians being influenced by this sickness consistently [1].

Specific CAD frameworks have been produced to help radiologists in recognizing aspiratory Tumors that demonstrate the presence of lung Tumor. Computer aided design frameworks when all is said in done comprise of three phases; pre-processing, feature extraction and characterization. Machine learning was enlivened by the human cerebrum's architecture. It is anticipated that deaths caused by disease will rise to 13.1 million continuously 2030. In Malaysia, as per the National Cancer Registry (NCR), the best five regular kinds of Tumor growth that influence the populace paying little mind to gender are colorectal, lung, cervix and nasopharynx [2].

Different sorts that are additionally influencing Indians incorporate liver Tumor and prostate disease. 21,773 cases were enlisted in NCR in the year 2017 that have been influenced by one kind of Tumor in India. Since the reason for disease is as yet obscure, early identification and treatment of Tumor is viewed as the most encouraging ways to deal with reducing the count of deaths [3-5].

With advancement in social insurance and therapeutic innovation and with the populace maturing and developing, the interest for human services is expanding. Prompting lines for patients to be analyzed and expanding strain on the well charge framework. Longer lines may prompt patients being analyzed in later phases of the ailment, causing enduring and expanded danger of mortality, which thus requires more assets and spending in the human services part. In any case, are more assets and more cash planned to the social insurance part the arrangement? Imagine a scenario where the social insurance division were digitalized in a more extensive degree, and consider the possibility that there would be self-ruling conclusion frameworks to help the radiologists [6-8].

Today, man-made brainpower (AI) and self-learning frameworks are broadly examined in the human services division, rendering both interest and distrust about these future advances. In any case, the medicinal services part need inventive and present day answers for turn out to be increasingly productive. Tumor growth is a typical infection, and lung disease is the most widely recognized tumor analyze on the planet. It is urgent for the survival of a patient to be analyzed in a beginning time of the tumor growth. The prior the tumor growth is distinguished and treated, the higher the survival-rate of the patient [9].

The finding of lung tumor is regularly founded on pictures of the lungs, for example, ordinary X-beam framework and CT checks. It is a troublesome and tedious errand to translate restorative pictures, and to analyze a patient utilizing pictures an accomplished radiologist is required. By executing self-ruling finding frameworks as choice help for radiologists, the two expenses for the medicinal services division and patients enduring can be decreased [10]. The point of this proposed work is to subsequently explore the likelihood of a grouping calculation to separate lung tumor tissue and typical lung tissue in CT examinations.

2. Related Work

Masood et al. (2020) developed a novel 3D Deep Convolutional Neural Network (3DDCNN)-based computer-aided decision support network for lung knob detection to assist radiologists. This structure used multi-Region Proposal Network (mRPN) and middle power projection to automate the selection of anticipated points of interest. The Framework outperformed the leading frameworks in its category and achieved a remarkable 98.7% affectability at 1.97 FPs per scan [11].

In order to categories lung CT image patches into 7 groups, including 6 unique ILD patterns and solid tissue, Anthimopoulos et al. (2016) suggested a sophisticated CNN. Extratextural lung designs may be used to properly teach the technique, and execution can be enhanced by a closer inspection of the delicate boundaries. The data show that cellular scenarios, which require an accurate depiction of the outer layer in addition to the primary request portrayal of power esteems, are the main root cause of the higher misclassification rate [12].

Jakimovski et al.'s pre-characterization of the pictures using the K-implies calculation enables the DNN to concentrate on the grouping of precisely sliced images. The additional convolution layer with edge honing channels, which is used to thoroughly search for cancerous development, is the next area of interest. With the help of the oncology office's clinical experts, the results were reviewed and classified as acceptable to determine malignancy. This structure generates computational cost due to the massive informational gathering [13].

On the basis of computed tomography data, Yu et al. (2020) showed how deep learning helped the “Adaptive Hierarchical Heuristic Mathematical Model (AHHMM)” forecast cellular breakdown in the lungs. The suggested AHHMM framework successfully foretells processed tomography examinations of lung cellular disintegration. The evaluation's discovery revealed that almost 90% of the images had been correctly recognised. These findings demonstrate the value of DNN in blister determination for classifying lung cell breakdown [14].

In order to reduce the computational complexity of CNN, Asuntha et al. (2020) suggested a revolutionary FPSOCNN (“Fuzzy Particle Swarm Optimization based Convolutional Neural Network”). The results of the trials demonstrate that the innovative FPSOCNN outperforms other techniques. This design foresees improvements in our understanding of the risk of aspiratory knobs, which will be important for the identification and management of lung cell disintegration [15].

A model for the distribution of lung cancer infection groups was put out by Chauhan et al. (2016) based on an effective technique that makes use of machine learning principles. An intuitive sickness forecast model based on PCA and LDA has been developed, but due to the system's continuous output images, more calculation time is needed [16].

Shakeel et al. (2020) use better deep neural organization and classifiers to analyze the cellular breakdown in the lungs. When the effectiveness of the framework is evaluated using the results of exploratory studies, the framework accurately detects the sickness. A better location division and feature determination method is required to accurately identify the deviation in cells that are developing normally and malignantly [17].

Wong et al. (2018) narrowed their attention on the process for the breakdown of cells in the lungs by classifying the data according to breath. In this framework's study, cross-approval and KNN were also utilized. At 84.4%, we finally achieved excellent accuracy. To handle the huge dataset, more updates are required [18].

The MV-KBC model was developed by Xie et al. (2019) to distinguish between benign and malignant lung screws on chest computed tomography through taking into consideration the knob appearance on nine view planes, the knob heterogeneity, and the use of a variable weighting scheme. Consequently, we may prepare our model from beginning to end. Results indicate that our model is more accurate than how existing techniques are currently doing on the LIDC-IDRI dataset [19].

Lung cancer detection methods based on SVM and RF have been proposed by Vikas et al. (2021). The chi-squared method is used in this procedure to choose the features. Chi-square feature selection is used both with and without the analysis. Recall, precision, and accuracy are additional metrics used by the framework to assess overall performance. Results show that this approach improves performance by reducing the amount of time needed for execution [20].

The summary of the related work is provided below. The existing research works used DL and ML techniques DNN, CNN, DDCNN, KNN, and SVM, etc. to predict lung cancer. But the discovery still has a gloomy side since it cannot yet predict lung cancer with high accuracy and little complexity. The suggested study has used firefly optimization to classify tumors in lung CT scan pictures better than the conventional neural network in order to address the aforementioned problems.

3. Proposed Framework

Figure 1. Provides the overall design of the recommended approach. Three crucial phases make up the structure of operation of the planned "deep learning" driven diagnosis with classification of system. Before training the firefly-optimized CNNs, the image preprocessing as well as augmentation procedure, the capsule driven saliency segments, the precise feature extraction utilizing the learning of transfer & the end step.

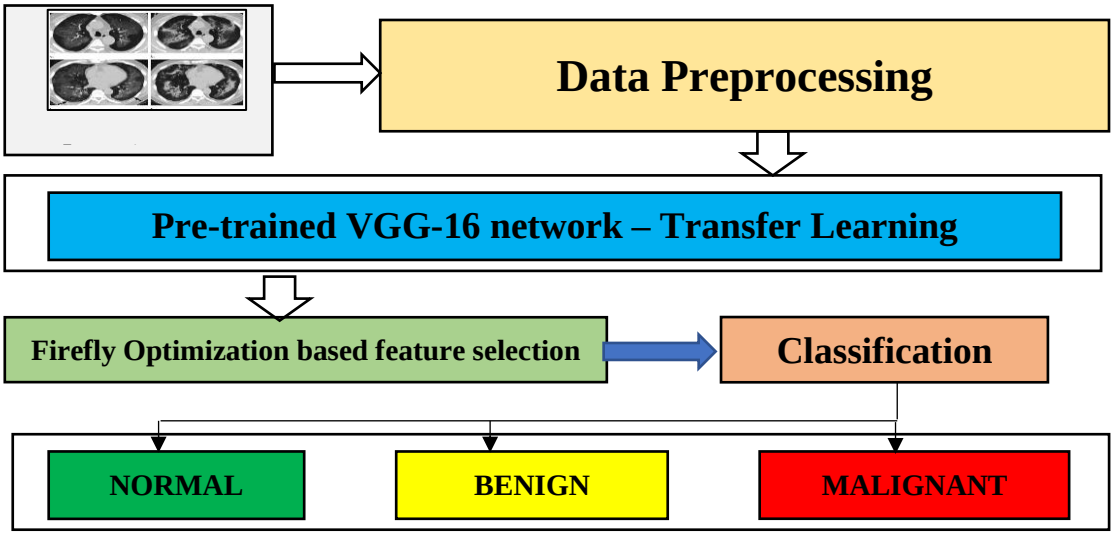

Figure 1. Working of proposed framework

3.1 Data Preprocessing

CT scans are distinguished utilizing the HOE technique as the first step. The image brightness as well as contrast are adjusted using this pre-processing step [21]. The following is the numerical expression of HOE used for image pre-processing:

$$I = Tn/P \quad (1)$$

Wherein Tn – "Number of pixels in N levels" N⇨[0,255]

P – "Total Number of pixels".

AMF is implemented to effectively denoise the images after preprocessing. Bilateral images that use AMF produce "clean, crisp, and artefact-free edges" in addition to enhancing visual appeal.

3.2 Transfer Learning For Feature Extractor

Transfer learning is used in this procedure to improve extraction of features and categorization. Transfer learning strategies are thought of as before trained CNNs which can be used to address various image categorization issues. Owing to its excellent precision and higher versatility, the Inception V3 modules has been used in this work. The unique inception-V3 weights, which were trained using ImageNet, take into account all images with a revised size of 1501503.

3.2.1 VGG-16 ARCHITECTURE

The VGG16 version of the VGG approach, frequently referred to as VGGNet, is used. A 16 layer CNN framework is used **[22].** The model named VGG16 can achieve a test reliability of 92.7% in ImageNet, a set of pictures containing over fourteen million trained shots across 1000 component classes. It is an entry created for the 2014 ILSVRC challenge that stands out.

By replacing sequences of the greater 33 filters with lower 33 filter sequences, VGG16 improves AlexNet. The kernel size of "AlexNet" is 11 for the first layer of convolution and 5 for the subsequent layer.

3.2.2 The Reasons beneath the VGG Model

The VGG model's evaluation version was created for the 2014 ImageNet's competition **[23].** They belonged to the VGG at Oxford.

This strategy differed in many of respects from earlier, successful iterations. First off, AlexNet utilised 1111 fields of reception with a 4 pixel pace while using just 33 with a 1 pixel pace. The 33 filters are combined to serve the purpose of a larger receptive field.

The decision functionalities are better and a network may merge more quickly when multiple smaller layers are employed instead of a single large layer. This is due to the presence of additional nonlinear activation layers.

Second, VGG's smaller convolutional filter reduces the risk of the network over-fitting during training exercises. The ideal filter size is 33 since smaller sizes can't capture information that comes from the left, right, up, or down. VGG is the most straightforward paradigm that may be employed to understand the spatial characteristics of a picture. Because there are consistently 33 convolutions, the network is easy to regulate.

3.2.3 VGG16 design

VGG16 represents a 16 layers deep NN, as its name would imply. The VGG16 networks is therefore quite huge by today's standards, having 138 million parameters total. But the simplicity of the VGGNet16 layout is its main appeal.

The VGGNet architecture incorporates the key elements of convolutional neural networks shown in Figure 2.

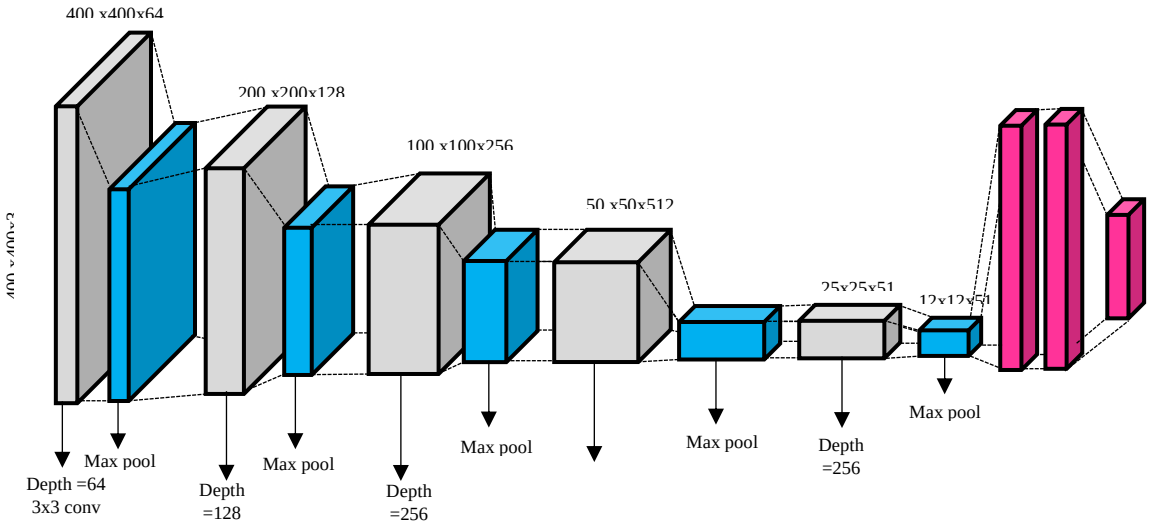

Figure 2. VGG design

Tiny convolution filters are the building blocks of VGG networks. Thirteen convolutional layers & three fully connected layers make up VGG16.

The VGG concept is described in more detail below:

- A 224224-pixel picture is entered into VGGNet. The model's creators were able to keep a constant image input size by eliminating a "224224 pixels" from the precise center of every picture presented for the ImageNet contest.
- Convolutional layers—the lowest imaginable receptive field is 33 and is provided by the VGG convolutional layer filter. VGG also employs an 11 convolution filter to linear transform the input.
- The next component is “AlexNet's” significant innovation for decreasing training times, the ReLU. ReLU is a function with linearity that produces an appropriate outcome for “positive inputs” & zero for “negative inputs”. After convolution, which is VGG has a “fixed convolution step of 1 pixel to preserve spatial resolution” (the stride number denotes the number of pixels that the filter itself "moves" to cover every pixel of the picture).
- Concealed layers—ReLU is used in place of local response standardization in all instances of the VGG design's layers that are concealed. The second strategy requires more memory and extends training sessions without enhancing overall accuracy.
- Pooling layers: To reduce the dimensionality and quantity of components in the feature mappings that every convolution phase generates, a layer for pooling is added after many convolutional layers. Pooling is crucial due to the swift rise in the quantity of viable filters from 64 to 128, 256 & ultimately 512 in the final levels.

The three layers of the VGGNet network are completely interconnected. 4096 channels are present on every single of the first two stages, while 1000 channels—one for every class—are present on the third layer.

3.3 Firefly Optimized Features:

This section discusses about firefly algorithm for the better feature selection from the VGG-16 (Pretrained Model).

3.3.1 Firefly Algorithm

The Firefly algorithm, which is regarded as a member of the clan of swarm intelligence techniques, was created by **[24].** During the summer months, it's common to watch the fireflies, also known as lighting bugs, blinking with light in the sky. The purpose of fireflies' flashing behavior is to either attract a potential mate or to protect themselves from predators. When a firefly is farther away from a brighter one, the strength of the light I receive likewise drops. However, as the distance grows, the air also has an impact on the light's intensity by absorbing it. As consequently, the value of light intensity and the value of fitness are directly related. To construct a working concept for the program, three assumptions must be made given the complexity of firefly natural behaviors. The following assumptions are made:

1. It was considered that all fireflies were unisex and that desire occurred between them regardless of sex.

2. Attractiveness decreases with increasing distance between fireflies and is roughly inversely correlated with brightness.

3. The objective function's workable solutions are used to calculate brightness or light intensity.

The suppositions make it abundantly evident that the intensity of light I(r) of fireflies has an inverse relationship to distance r since it diminishes as distance increases and light is also absorbed while it travels through the air. The coefficient of light absorption is represented by the symbol y. Equation (4.16) displays the fluctuation of firefly light intensity I(r) in relation to distance r.

$$I(r) = I_0 e^{-yr2} \quad (2)$$

Where I_0 ⇨ “initial value of intensity at the source and the attractiveness parameter”

β can be given in ways as shown

$$\beta(r) = \beta 0 e^{-yr2} \quad (3)$$

At the initial distance of zero, attractive variables are denoted as $\beta 0$

The equation below provides a behavior rule for estimating firefly positions.

$x_{i+1}=x_i+ \beta(r(i,j))(xj - xi) + AE$ (4)

Where A ⇨ "randomization factor" & E ⇨ "random number vector" x_1i⇨ " i[th] position of the firefly" & x_{i+1} ⇨ "the value of attraction".

3.3.2 Recommended Firefly Based Feature Selection

The following computational framework is used by the Firefly Algorithm, which uses synergic local search and is inspired by the physiological and social characteristics of a genuine firefly (Lampyridae).

The characteristics found in the data set under observation are used to initialize a search space S of m dimensions. Each feature in this binary feature space can either be present either one (1) or absent (0), increasing the number of alternative subgroups of the features exponentially. N fireflies are randomly distributed around the space, each with an intensity of Ii and a position indicated by xi. Each firefly's luminosity is connected to an objective value f(x) in the following way: BFA focuses on the formulation of attraction and the fluctuation of light intensity as the two variables for modeling firefly behavior. While the illumination intensity I(r) changes given in equation (5) according to the following equation, the light intensity I(S) of a firefly representing the best feature subset s corresponds to the fitness function's value as I(S) αf(s).

$$I(r) = I_0 e^{-\gamma r^2} \quad (5)$$

where I_0⇨ "the light intensity of the source, & absorption is approximated using the fixed light absorption coefficient γ".

Combining the consequences of the inverse square law with a Gaussian form approximation of absorption prevents a singularity at r=0 in the statement $1/_{r^2}$. Firefly attraction is inversely correlated with light intensity I_r. For the purpose of to describe the attractiveness, β a definition of an equation resembling Equation (6).

$$\beta = \beta_0 e^{-\gamma r^2} \quad (6)$$

Where β_0 ⇨ "attractiveness at r = 0".

Any two fireflies can be separated from one another by the Euclidean distance, which is expressed in equation (7):

$$r_{ij} = \| S_i - S_j \| \sqrt{\sum_{k=1}^{k=n}(S_{ik} - S_{jk})^2} \quad (7)$$

Where n ⇨ "the dimensionality of the problem". A second, more alluring firefly, j, is drawn to the motion of the i[th] firefly. The equation (8) that follows is employed in this way:

$$S_i = S_i + \beta_0 e^{-\gamma r_{ij}^2}(S_j - S_i) + \alpha\epsilon_i \quad (8)$$

Where ϵ_i⇨ "random number drawn from the Gaussian distribution".

When β0=0, just the random walk determines how far you advance. The parameter, on another hand, significantly affects the rate of convergence. The following equations (9) and (10) are used to translate the challenge to a discrete space since feature selection entails finding the best solutions in the binary searching space

$$.S_i^k(t+) = \begin{cases} (S_i^k(t))^{-1} & if\ rand < T(S_i^k(t)) \\ S_i^k(t) & if\ rand \geq T(S_i^k(t)) \end{cases} \quad (9)$$

$T(S_t^k)$ is calculated using:

$$T(x) = |\text{erf}(\frac{\sqrt{\pi}}{2}x)| = |\frac{\sqrt{2}}{\pi}\int_0^{\frac{\sqrt{\pi}x}{2}} e^{-t^2}dt| \quad (10)$$

Where $S_i^k(t)$ ⇨ "the position of firefly $i$at time t in the k th dimension". We employ the error function depicted in equation (9) because it has been successfully used to transfer continuous data into a separate binary environment.

3.3.3 FEATURE SELECTION BASED ON THE FIREFLY'S FITNESS FUNCTION

By excluding redundant characteristics and including important ones, the feature subset selecting seeks to achieve binary optimization of the fitness function. Optimizing the fitness function serves two purposes:

- Reduction of Features

- Increase classification precision

The aforementioned fitness function is defined in equation (11):

$$\rho(b,d) = A(b,d) - \emptyset(b) \quad (11)$$

where ρ ⇨ "fitness function", b ⇨ "the feature vector", d ⇨ "the dataset", A ⇨ "classification accuracy", $\emptyset$ ⇨ "penalty function over a feature subset b" defined in equation (12):

$$\emptyset(b) = \frac{\lambda|x|}{|N|} \quad (12)$$

$|x|$ ⇨ "total number of features in the dataset", $|N$ ⇨ "total number of features in the selected subset" & λ ⇨ "parameter corresponding to the weight given to the penalty function"

3.4 Classification Layers

After the selection features, then these are feed for training the networks. These training networks are constructed based on the hyper parameters as shown in the Table I. For achieving the more classification performance, the ADAM optimizer is incorporated to train the dense neural networks.

Table 1: Hyper parameters for constructing the dense NN

S.No	Specifications	Values
01	Epochs no	100
02	Rate of learning	100%
03	Batch size	20
04	Optimization Iterations	19
05	No of concealed nodes	78

4. Results and Discussion

The cancer imaging archives' ("https://wiki.cancerimagingarchive.net/display/Public/LIDC-IDRI") lung CT pictures are used in the experiments. The database consists of 1018 lung computed tomography (CT) images that have been collected from the National Cancer Institute and linked to proteomic and genetic clinical information. In this study, benign and malignant nodules are classified in all training images. A benign nodule is one with a malignancy score under 3, while a malignant lesion is one with a malignancy score over 3. The pulmonary nodules with a malignancy score of 3 are eliminated to eliminate sample ambiguity. The programme NBIA Retriever is used to convert TCIA format data into DICOM image data, which may subsequently be processed further.

An Intel I7 processor, a 2GB NVIDIA Geoforce K+10 GPU, 16GB of RAM, and a 2TB hard drive running at 3.0 GHz are used to power the entire experiment. With the Keras API and Tensorflow 1.8, the suggested architecture is put into practise. With Python 3.8 programming, all of the programmes are implemented in the Anaconda environment.

- **PERFORMANCE METRICS AND EVALUATION:**

The six CNN layers are used in the suggested architecture to improve the categorization of cancer cells in lung pictures. The datasets used to train and test the network are shown in Table II.

Table 2: Number of datasets used overall (after augmentation) to train and test the proposed network

Sl.no	Total Number of Images	Training Data(%)	Testing Data(%)
01	78090	70	30

In order to evaluate the success of the proposed design, metrics such as accuracy, sensitivity, specificity, recall, and f1-score are created. Table III displays the equations for the metrics used to evaluate the proposed design.

Table 3: Calculating Performance Metrics Using Mathematical Expressions

SL.NO	Performance Metrics	Mathematical Expression
01	Accuracy (A_y), (R_l) (S_f) (P_n) (F_s)	$\frac{TP+TN}{TP+TN+FP+FN}$
02	Sensitivity or recall (R_l)	$\frac{TP}{TP+FN}$ x100
03	Specificity (S_f)	$\frac{TN}{TN+FP}$
04	Precision (P_n)	$\frac{TN}{TP+FP}$
05	F1-Score (F_s)	$2.\frac{Precison * Recall}{Precision + Recall}$

"TP is True Positive Values, TN is True Negative Values, FP is False Positive and FN is False negative values"

The validation findings from the proposed tumor predictor and various depth networks are highlighted in this section. For the initial iteration, the verification data used for testing has been divided into four separate folds: "(i) confusion matrix; and (ii) ROC". By computing the various performance indicators listed in Table IV, the projected architecture is then contrasted with other widely used transfer learning models, including "CNN [25], Resnets-100 [26], Resnets-150 [27], InceptionV3 [28], Google-Net [29], Mobile-Net [30] Densenet-169 [31] and segCaps [32]". In order to solve the imbalance issues, the suggested method is evaluated using random 900Lung CT scan pictures that contain 50% benign, 50% normal, and 50% malignant tissue.

.

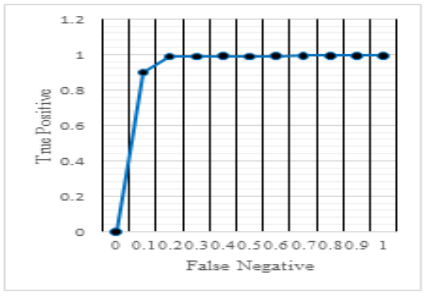

(a)

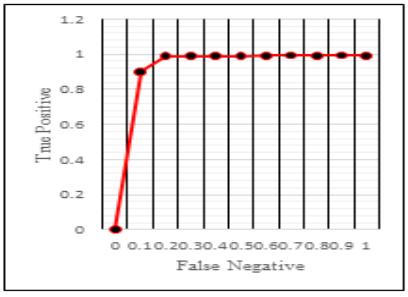

(b)

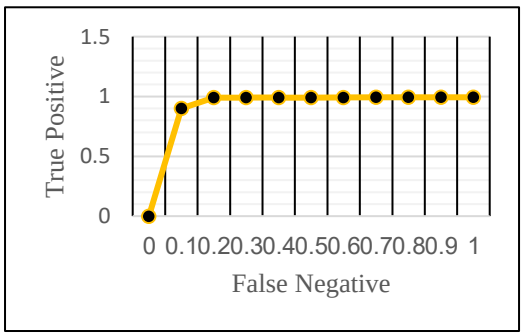

(c)

Figure 3. "ROC curves" – recommended framework in detecting a) Normal b) Begnin c) Malignant

Table 4: Confusion matrix – recommended framework employing 900 random tested pictures

CLASSES	BEGNIN	MALIGNANT	NORMAL
BEGNIN	295	01	04
MALINGNANT	01	296	03
NORMAL	01	03	296

Table 5

Algorithm Details	Performance Metrics				
	A_y (%)	R_l (%)	S_f (%)	P_n (%)	F_s (%)
CNN [25]	81.3	71.4	77.6	73.5	79.4
Resnets-100 [26]	82.4	81.3	81.45	80.1	82.3
Resnets-150 [27]	83.1	82.1	85.0	83.1	81
Inception V3 [28]	84.68	84.7	85.623	85.5	84.5
Google-Net [29]	82.1	81.2	83.1	81.2	82.1
Mobile Nets [30]	81.4	81.5	82.5	84.2	86.0
Densenet-169 [31]	83.4	81.7	84.8	83.3	85.6
SegCaps [32]	90.0	89.8	90.8	90.6	89.7
Proposed Framework	98.95	98.85	98.85	98.75	98.85

Table 5 various deep learning techniques – performances statistics in predicting the normal LUNG CT pictures

Table 6

Algorithm Details	Performance Metrics				
	A_y (%)	R_l (%)	S_f (%)	P_n (%)	F_s (%)
CNN [25]	79	71.5	78.4	76	74.2
Resnets-100 [26]	82.4	82.53	81.3	81.7	82.32
Resnets-150 [27]	85.3	82.1	85.7	85.3	81.2
Inception V3 [28]	88.8	87.53	84.3	87.3	81.34
Google-Net [29]	82.5	81.3	83.1	81.5	82.4
Mobile Nets [30]	82.2	82.2	85.2	82.5	82.66
Densenet-169 [31]	85.8	88.7	84.5	84.8	86.7
SegCaps [32]	90.2	91.8	90.6	91.3	89.67
Recommended Framework	98.95	98.85	98.85	98.9	98.89

Table 6 Performance of several deep learning architectures, including accuracy, sensitivity, specificity, precision, and recall, in identifying malignant cancers in Lung CT Images

Table 7

Algorithm Details	Performance Metrics				
	A_y (%)	R_l (%)	S_f (%)	P_n (%)	F_s (%)
CNN [25]	79	79	77.6	78.8	71.4
Resnets-100 [26]	82.3	81.3	81.45	82.4	82.2
Resnets-150 [27]	85.22	82.2	85.,0	84.9	83
Inception V3 [28]	88.78	83.67	88.623	84.3	82.5
Google-Net [29]	82.3	81.4	83.2	81.1	82.5
Mobile Nets [30]	86.5	83.6	84.5	85.2	84.0
Densenet-169 [31]	83.784	81.9	85.8	81.9	80.2
SegCaps [32]	92.0	90.83	91.8	91.0	92.6
Proposed Framework	98.95	98.85	98.85	98.75	98.85

Table 7 the accuracy, sensitivity, specificity, precision, and recall of various deep learning architectures in identifying malignant cancers in Lung CT images

The suggested framework's “ROC curve” (Figure 3) and “confusion matrix” (Figure 4) for classifying CT scan lung pictures. The performance gained using the proposed framework in comparison to other widely used methods is highlighted in Tables IV, V, & VI. Table IV reveals that the recommended method has showed “98.95% accuracy in recognizing normal”, benign, and malignant CT pictures with “98.85% sensitivity, 98.76% precision, and a high f1score of 98.85%”. From table V, it is apparent that efficiency in spotting cancerous pictures is similar. Tables V & VI make it evident that the presented network has demonstrated a greater detection ratio employing the merger of saliency with capsule and optimal transfer learning than the conventional approach.

5. Conclusion and Future Scope

The purpose of proposed framework is to use CT scan images of the lungs to identify and categorize malignant and early cancer cells. This study makes use of feature extraction based on transfer learning to categorize cancer cells. In order to improve classification accuracy, the suggested architecture makes use of a firefly-based feature selection method. The provided tumor identification method has been evaluated utilizing the “Tensorflow 1.8 tool with the Keras API”, and a number of performance measures, includes “accuracy, precision, recall, specificity & f1-score”, have been produced and examined. The investigation data demonstrates that the suggested design obtained the excellent results compared to alternative conventional structures and the better peak outcomes. More thorough testing will be required in the future and use greater clinical datasets. Furthermore, the recommended algorithm necessarily to be improved in regards to computing difficulty will be important for more correctly analyzing and identifying tumor cells from the perspective of a radiologist.

References

[1] S. Das and S. Majumder, "Lung Cancer Detection Using Deep Learning Network: A Comparative Analysis," 2020 Fifth International Conference on Research in Computational Intelligence and Communication Networks (ICRCICN), Bangalore, India, 2020, pp. 30-35, doi: 10.1109/ICRCICN50933.2020.9296197.

[2] R. Tekade and K. Rajeswari, "Lung Cancer Detection and Classification Using Deep Learning," 2018 Fourth International Conference on Computing Communication Control and Automation (ICCUBEA), Pune, India, 2018, pp. 1-5, doi: 10.1109/ICCUBEA.2018.8697352.

[3] B. S, P. R and A. B, "Lung Cancer Detection using Machine Learning," 2022 International Conference on Applied Artificial Intelligence and Computing (ICAAIC), Salem, India, 2022, pp. 539-543, doi: 10.1109/ICAAIC53929.2022.9793061.

[4] M. Praveena, A. Ravi, T. Srikanth, B. H. Praveen, B. S. Krishna and A. S. Mallik, "Lung Cancer Detection using Deep Learning Approach CNN," 2022 7th International Conference on Communication and Electronics Systems (ICCES), Coimbatore, India, 2022, pp. 1418-1423, doi: 10.1109/ICCES54183.2022.9835794.

[5] M. Thaseen, S. K. UmaMaheswaran, D. A. Naik, M. S. Aware, P. Pundhir and B. Pant, "A Review of Using CNN Approach for Lung Cancer Detection Through Machine Learning," 2022 2nd International Conference on Advance Computing and Innovative Technologies in Engineering (ICACITE), Greater Noida, India, 2022, pp. 1236-1239, doi: 10.1109/ICACITE53722.2022.9823854.

[6] M. Marathe and M. Bhalekar, "Detection of Lung Cancer using CT Scans with Deep Learning Approach," 2022 7th International Conference on Communication and Electronics Systems (ICCES), Coimbatore, India, 2022, pp. 1026-1031, doi: 10.1109/ICCES54183.2022.9835901.

[7] G. V. Saji, T. Vazim and S. Sundar, "Deep Learning Methods for Lung Cancer Detection, Classification and Prediction - A Review," 2021 Fourth International Conference on Microelectronics, Signals & Systems (ICMSS), Kollam, India, 2021, pp. 1-5, doi: 10.1109/ICMSS53060.2021.9673598.

[8] B. Jehangir, S. R. Nayak and S. Shandilya, "Lung Cancer Detection using Ensemble of Machine Learning Models," 2022 12th International Conference on Cloud Computing, Data Science & Engineering (Confluence), Noida, India, 2022, pp. 411-415, doi: 10.1109/Confluence52989.2022.9734212.

[9] R. P.R., R. A. S. Nair and V. G., "A Comparative Study of Lung Cancer Detection using Machine Learning Algorithms," 2019 IEEE International Conference on Electrical, Computer and Communication Technologies (ICECCT), Coimbatore, India, 2019, pp. 1-4, doi: 10.1109/ICECCT.2019.8869001.

[10] A. Rehman, M. Kashif, I. Abunadi and N. Ayesha, "Lung Cancer Detection and Classification from Chest CT Scans Using Machine Learning Techniques," 2021 1st International Conference on Artificial Intelligence and Data Analytics (CAIDA), Riyadh, Saudi Arabia, 2021, pp. 101-104, doi: 10.1109/CAIDA51941.2021.9425269.

[11] A. Masood, P. Yang, B. Sheng, H. Li, P. Li et al., "Cloud-based automated clinical decision support system for detection and diagnosis of lung cancer in chest CT," IEEE Journal of Translational Engineering in Health and Medicine, vol. 8, pp. 1–13, 2020.

[12] M. Anthimopoulos, S. Christodoulidis, L. Ebner, A. Christe and S. Mougiakakou, "Lung pattern classification for interstitial lung diseases using a deep convolutional neural network," IEEE Transactions on Medical Imaging, vol. 35, no. 5, pp. 1207–1216, 2016.

[13] G. Jakimovski and D. Davcev, "Using double convolution neural network for lung cancer stage detection," Applied Sciences, vol. 9, no. 3, pp. 427. 2019.

[14] H. Yu, Z. Zhou and Q. Wang, "Deep learning assisted predict of lung cancer on computed tomography images using the adaptive hierarchical heuristic mathematical model," IEEE Access, vol. 8, pp. 86400–86410, 2020.

[15] A. Asuntha and A. Srinivasan, "Deep learning for lung cancer detection and classification," Multimedia Tools and Applications, vol. 79, pp.7731–7762, 2020.

[16] D. Chauhan and V. Jaiswal, "An efficient data mining classification approach for detecting lung cancer disease," in Proc. International Conference on Communication and Electronics Systems, Coimbatore, India, pp. 1–8, 2016.

[17] P. M. Shakeel, M. A. Burhanuddin and M. I. Desa, "Automatic lung cancer detection from CT image using improved deep neural network and ensemble classifier," Neural Computing and Applications, 2020.

[18] D. M. Wong, C. Y. Fang, L. Y. Chen, C. I. Chiu, T. I. Chou et al., "Development of a breath detection method based e-nose system for lung cancer identification," in Proc. IEEE International Conference on Applied System Invention, Chiba, Japan, pp. 1119–1120, 2018.

[19] Y. Xie, Y. Xia, J. Zhang, Y. Song, D. Feng et al., "Knowledge-based collaborative deep learning for benign-malignant lung nodule classification on chest CT," IEEE Transactions on Medical Imaging, vol. 38, no. 4, pp. 991–1004, 2019.

[20] Vikas and P. Kaur, "Lung cancer detection using chi-square feature selection and support vector machine algorithm," International Journal of Advanced Trends in Computer Science and Engineering, vol.10, no.3, pp.2050-2060, 2021.

[21] Fei Wang et al., "Two-dimensional dense-arrayed probe-cards with a hoe-shaped probing-tip micromachining technique," 2008 IEEE 21st International Conference on Micro Electro Mechanical Systems, Wuhan, 2008, pp. 343-346, doi: 10.1109/MEMSYS.2008.4443663.

[22] J. Tao, Y. Gu, J. Sun, Y. Bie and H. Wang, "Research on vgg16 convolutional neural network feature classification algorithm based on Transfer Learning," 2021 2nd China International SAR Symposium (CISS), Shanghai, China, 2021, pp. 1-3, doi: 10.23919/CISS51089.2021.9652277.

[23] J. B. Hopson et al., "Pre-training and Transfer Learning for Training Set Reduction and Improving Automated Assessments of Clinical PET Image Quality," 2021 IEEE Nuclear Science Symposium and Medical Imaging Conference (NSS/MIC), Piscataway, NJ, USA, 2021, pp. 1-3, doi: 10.1109/NSS/MIC44867.2021.9875796.

[24] S. Goel and V. K. Panchal, "Performance evaluation of a new modified firefly algorithm," Proceedings of 3rd International Conference on Reliability, Infocom Technologies and Optimization, Noida, India, 2014, pp. 1-6, doi: 10.1109/ICRITO.2014.7014717.

[25] R. Maeda et al., "Predicting the severity of Neonatal Chronic Lung Disease from chest X-ray images using deep learning," 2022 IEEE International Conference on Systems, Man, and Cybernetics (SMC), Prague, Czech Republic, 2022, pp. 1543-1547, doi: 10.1109/SMC53654.2022.9945486.

[26] R. Shethwala, S. Pathar, T. Patel and P. Barot, "Transfer Learning Aided Classification of Lung Sounds-Wheezes and Crackles," 2021 5th International Conference on Computing Methodologies and

Communication (ICCMC), Erode, India, 2021, pp. 1260-1266, doi: 10.1109/ICCMC51019.2021.9418310.

[27] A. Serener and S. Serte, "Deep learning to distinguish COVID-19 from other lung infections, pleural diseases, and lung tumors," 2020 Medical Technologies Congress (TIPTEKNO), Antalya, Turkey, 2020, pp. 1-4, doi: 10.1109/TIPTEKNO50054.2020.9299215.

[28] A. Gupta and A. Kumar, "Deep-Learning Based Hybrid Model For The Classification of Lung Diseases," 2022 4th International Conference on Artificial Intelligence and Speech Technology (AIST), Delhi, India, 2022, pp. 1-4, doi: 10.1109/AIST55798.2022.10065198.

[29] P. Rattanawin, T. Pakinsee and P. Songmuang, "A GoogLeNet Performance Approach for COVID-19 Detection using Chest X-ray Images," 2023 15th International Conference on Knowledge and Smart Technology (KST), Phuket, Thailand, 2023, pp. 1-5, doi: 10.1109/KST57286.2023.10086817.

[30] V. Vaityshyn, H. Porieva and A. Makarenkova, "Pre-trained Convolutional Neural Networks for the Lung Sounds Classification," 2019 IEEE 39th International Conference on Electronics and Nanotechnology (ELNANO), Kyiv, Ukraine, 2019, pp. 522-525, doi: 10.1109/ELNANO.2019.8783850.

[31] K. Nair, A. Deshpande, R. Guntuka and A. Patil, " Analysis X-Ray Images to detect lung diseases using Densenet-169 technique," 2022.

[32] P. Bhatia, A. Sinha, S. P. Joshi, R. Sarkar, R. Ghosh and S. Jana, "Automated Quantification of Inflamed Lung Regions in Chest CT by UNet++ and SegCaps: A Comparative Analysis in COVID-19 Cases," 2022 44th Annual International Conference of the IEEE Engineering in Medicine & Biology Society (EMBC), Glasgow, Scotland, United Kingdom, 2022, pp. 3785-3788, doi: 10.1109/EMBC48229.2022.9870901.